# X-ray absorption spectroscopy of iron at multimegabar pressures in laser shock experiments

M Harmand, A Ravasio, S Mazevet, J Bouchet, A Denoeud, F Dorchies, Y Feng, C Fourment, E Galtier, Jerôme Gaudin, et al.

# X-ray absorption spectroscopy of iron at multimegabar pressures in laser shock experiments

M. Harmand,[1,2,*] A. Ravasio,[1] S. Mazevet,[3] J. Bouchet,[4] A. Denoeud,[1] F. Dorchies,[5] Y. Feng,[6] C. Fourment,[5] E. Galtier,[6] J. Gaudin,[5] F. Guyot,[2] R. Kodama,[7] M. Koenig,[1] H. J. Lee,[6] K. Miyanishi,[7] G. Morard,[2] R. Musella,[3] B. Nagler,[6] M. Nakatsutsumi,[8] N. Ozaki,[7] V. Recoules,[4] S. Toleikis,[9] T. Vinci,[1] U. Zastrau,[6,10] D. Zhu,[6] and A. Benuzzi-Mounaix[1,3]

[1]*LULI, Ecole Polytechnique, CNRS, CEA, UPMC, Palaiseau, France*
[2]*IMPMC, CNRS, UPMC, MNHN, IRD, Paris, France*
[3]*LUTH, Observatoire de Paris, CNRS, Université Paris Diderot, Meudon, France*
[4]*CEA-DAM-DIF, Arpajon, France*
[5]*CELIA, Univ. Bordeaux, CEA, CNRS, Talence, France*
[6]*LCLS, SLAC Stanford, California, USA*
[7]*Graduate School of Engineering, Osaka University, Osaka, Japan*
[8]*European XFEL, GmbH, Albert-Einstein-Ring 19, 22671 Hamburg, Germany*
[9]*FLASH, Desy, Hamburg, Germany*
[10]*Institute for Optics and Quantum Electronics, Friedrich-Schiller-University of Jena, Germany*

(Received 3 December 2014; revised manuscript received 12 May 2015; published 29 July 2015)

Taking advantage of the new opportunities provided by x-ray free electron laser (FEL) sources when coupled to a long laser pulse as available at the Linear Coherent Light Source (LCLS), we have performed x-ray absorption near-edge spectroscopy (XANES) of laser shock compressed iron up to 420 GPa (±50) and 10 800 K (±1390). Visible diagnostics coupled with hydrodynamic simulations were used to infer the thermodynamical conditions along the Hugoniot and the release adiabat. A modification of the pre-edge feature at 7.12 keV in the XANES spectra is observed above pressures of 260 GPa along the Hugoniot. Comparing with *ab initio* calculations and with previous laser-heated diamond cell data, we propose that such changes in the XANES pre-edge could be a signature of molten iron. This interpretation then suggests that iron is molten at pressures and temperatures higher than 260 GPa (±29) and 5680 K (±700) along the principal Fe Hugoniot.

DOI: 10.1103/PhysRevB.92.024108 PACS number(s): 64.70.D−, 61.05.cj, 62.50.Ef, 91.35.Lj

Several important planetary features such as heat flux, convection within the core, and hence geodynamo and secular cooling are intimately related with core temperature profiles, which, in turn, critically hinge on the melting curve of constituent materials. As a reference, the melting curve of pure iron, the main constituent of Earth's and Earth-like planetary cores, is of a critical importance and has been the purpose of numerous experimental and theoretical works [1–12]. It remains up to now largely uncertain mainly due to experimental difficulties in reaching and detecting melting of iron at terrestrial inner core boundary (ICB) conditions, where the pressure is of 330 GPa. A significant advance was recently accomplished by coupling laser-heated diamond-anvil-cell (DAC) compression to x-ray diffraction. This latest attempt provided measurements of molten iron up to 150 GPa and in agreement with recent *ab initio* calculations [4]. However, laser-heated DAC techniques only give access to a limited pressure and temperature range.

Dynamic compression offers the possibility to provide measurement of iron at pressures and temperatures close to the ICB conditions [8–13] and beyond, as needed for the modeling of planets larger than the Earth. However, previous dynamic compression measurements of the solid-liquid transition along the shock Hugoniot have shown important discrepancies [8–12]. As a result, the actual melting temperature of iron measured in dynamic compression experiments is showing a variation of more than 2000 K around 250 GPa. Because melting measurements using laser-induced dynamic compression were inferred indirectly using self-emission diagnostics on the surface of the shock front [8–10] or sound velocity measurements [11,12], overheating [5] and transient phases occurring before melting [6,7] were brought forward to explain such discrepancies. The overall difficulty in diagnosing unambiguously the solid-liquid transition within the short time scales involved in a dynamical process is an open issue that steamed the iron controversy. In addition to the difficulty in measuring temperature during dynamic compression, there is an important need to get structural information *in situ* during shock compression in order to identify a solid or liquid state of iron.

X-ray absorption near-edge structure (XANES) using synchrotron radiation was recently used with diamond-anvil-cell (DAC) compression to detect liquid iron up to 78 GPa as well as the bcc-hcp transition at 14 GPa [14,15]. In addition, signatures of molten iron in the XANES spectra were predicted using first-principles simulations [16,17]. Following recent progresses using XANES spectroscopy in dynamical experiments [18–20], we used this diagnostic to determine whether similar signatures could exist along the principal Hugoniot. Compared to x-ray diffuse scattering [4], the x-ray absorption technique offers the advantage of a higher cross section and therefore requires a lower photon number and thinner samples that are easier to compress homogeneously. It requires broadband x-ray sources and has been coupled to laser based dynamic compression only recently [13,18–20]. These latter experiments were using ps secondary x-ray sources either limited to few keV when using $M$-band emission [21] or requiring ultrahigh energy lasers (40 beams at the Omega facility [13]). Here we report the XANES spectra of iron at

*marion.harmand@impmc.upmc.fr

 

pressure and temperature conditions close to the ICB in the Earth and beyond, by coupling ultrafast time resolved x-ray absorption diagnostics using an x-ray free electron laser (FEL) with laser-induced dynamic compression techniques.

## I. DESCRIPTION OF THE EXPERIMENTAL SETUP

The experiment has been performed at the recently commissioned MEC (Matter in Extreme Conditions) instrument at the Linac Coherent Light Source (LCLS) in Stanford, CA, USA. Figure 1 shows the experimental setup that we used to investigate the state of iron along the principal shock Hugoniot [22]. To generate a shock, two long laser pulses (532 nm, 3 ns, from 2 to 7 J per pulse) were focused down to a 200 $\mu$m spot size on iron targets leading to intensities of $10^{12-13}$ W/cm$^2$. The targets consisted of multilayer samples made of CH/Cu/Fe/Cu/CH. With this particular design, the two Cu layers keep the iron sample in a strong compression as long and uniform as possible. The thickness of this first CH layer was chosen to optimize the ablation and to minimize x-ray radiation from the laser-produced coronal plasma. The strong impedance mismatch between the CH ablator and copper (and then iron) allowed us to get high pressures even though we had a relatively low energy laser [23]. The ~80 fs, ~3 mJ, 7.1 keV FEL beam was used to probe the compressed matter. Indeed, the FEL pulse duration is shorter than the processes involved and than the time over which uniform high pressures and temperatures are maintained (here typically on the order of few hundreds of picoseconds). The x-ray FEL brightness ($10^{12-13}$ photons/pulses) increases the flexibility of the target design by allowing the use of multilayers and high absorbing materials. By probing shocked iron at different times between the optical pump laser and the x-ray FEL (from 2 to 20 ns delays) and by using different laser intensities, we scanned the phase diagram of iron over a large domain along the Hugoniot, up to 420 GPa and along the release adiabat, down to 12 GPa.

Recently our experimental team has demonstrated the possibility to use x-ray FEL radiation to perform XANES

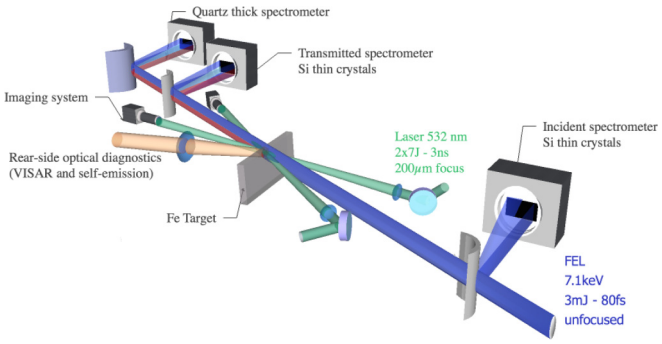


FIG. 1. (Color online) Two lasers are focused on the multilayer iron sample while the unfocused LCLS beam probes the compressed sample within femtosecond times scales. A first spectrometer measures the incident beam while two different spectrometers are detecting the transmitted beam allowing XANES measurements with two different methods. On the rear side of the target, optical diagnostics (VISAR and SOP) have been installed allowing the shot-to-shot measurement of the thermodynamical conditions when compared with hydrodynamical simulations.

spectroscopy over few tens of eV, restricted to the FEL spectral bandwidth of few percent, around an absorption edge. This required an accumulation over few tens of single shots [24]. Here we use simultaneously two different methods based on shot-to-shot measurement of the incident spectra (see Fig. 1). The first one uses bent quartz crystals with the unfocused FEL so that spectrometers are angularly dispersive along the horizontal direction but preserve the spatial information in the vertical direction. Coupled with a half-target design in the first method, only part of the beam goes through the sample while the remaining part of the beam is used for obtaining a reference spectrum or measuring the relative intensity fluctuation between spectrometers if existing. The extraction procedure of the XANES spectra associated with that method is further detailed in [24]. The second method consists of using thin identical Si crystals [25] placed symmetrically before and after the sample to directly measure the incident and transmitted spectra. By using an attenuated and unfocused FEL we also ensure that the x-ray photon intensity is too low to damage the spectrometers or the sample itself. Due to the sharp spectral features of the FEL source [24,25] we accumulated several single-shots measurements to obtain a XANES spectrum extending 30 eV beyond the iron $K$ edge.

In parallel, a set of two rear side diagnostics was implemented to check shot-to-shot the spatial homogeneity of the shock and to determine the shock velocities (see Fig. 2). From two VISARs (velocity interferometer system for any reflector) and a SOP (streaked optical pyrometer) we were able to measure, with a good precision of around 5%, the mean shock velocity in the rear side CH layer using the shock transit time and the initial thickness. Here the SOP was used to measure the shock transit time, as an additional and independent diagnostic to the VISAR, and did not allow us to measure directly the temperature. In addition and for high laser intensity, VISARs gave also the time-resolved shock velocity in CH ($\geqslant$13 km/s when metallization occurs in CH at pressures higher than 1 Mbar [26], see Fig. 2). For shots at lower intensities, for which the pressure is lower than 1 Mbar and plastic is opaque, the VISAR gave us the shock time transit (and then the mean shock velocity) thanks to ghost fringe disappearance when the shock breaks out in the void from the rear side of the CH layer.

## II. EXPERIMENTAL RESULTS AND ANALYSIS

### A. Determination of the probed thermodynamic conditions

In such a pump-probe experiment, an important difficulty is to infer thermodynamic conditions (pressure and temperature) of the iron sample at the time of the x-ray probe. To achieve this, we coupled VISAR and SOP measurements with hydrodynamic simulations. This is obtained by adjusting the effective laser intensity in the simulations to reproduce the shock velocity measured with the VISAR and the shock arrival time measured by the VISAR and SOP (see Fig. 2). This method has been validated previously in various experimental works [18,27]. In the present case, we find an average effective intensity of $9\times10^{12}$ W/cm$^2$ for shots using two beams (14 J in total). This is consistent with the specifications of the nanosecond laser taking into account losses of energy due

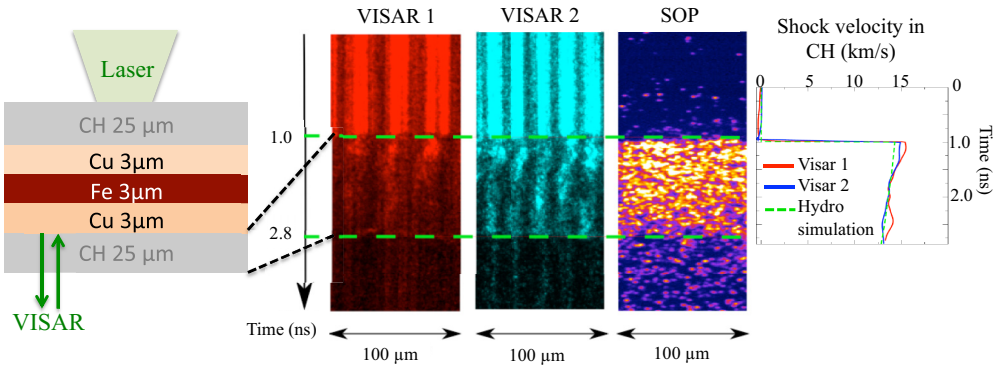


FIG. 2. (Color online) A zoom of the multilayer target is displayed with images from the two VISAR and the SOP measurements obtained at intensities of $9\times10^{12}$ W/cm$^2$. For such intensities, the backside CH layer metallizes and allows the measurements of the instantaneous shock velocity from the two VISARs. On the right, we show the corresponding instantaneous velocity from the two VISARS, overlaid with the shock velocity from hydrodynamic simulations to extract the pressure and the temperature. For lower intensity, we used the shock transit time from the two VISARS and the SOP detectors.

to the phase plates. The efficiency of this approach clearly relies however on the equation of states (EOS) used in the hydrodynamical simulations. For iron, various EOS have been tabulated over the years. In Fig. 3 we see the Hugoniot generated with the SESAME 2140 [28], the SESAME 2150 [29], and the Bushman-Lomonosov-Fortov (BLF) [30]. The most recent EOS SESAME table (2150) shows a solid-liquid transition preceded by a solid-solid transition between an extended face centered cubic (fcc) and hcp phases while the BLF EOS shows a melting transition that occurs at much higher temperatures than the SESAME 2150. The SESAME 2140 does not include solid-liquid phase transition and was therefore not considered for the present analysis. In the continuation of the recent results available for iron [4], we thus generated

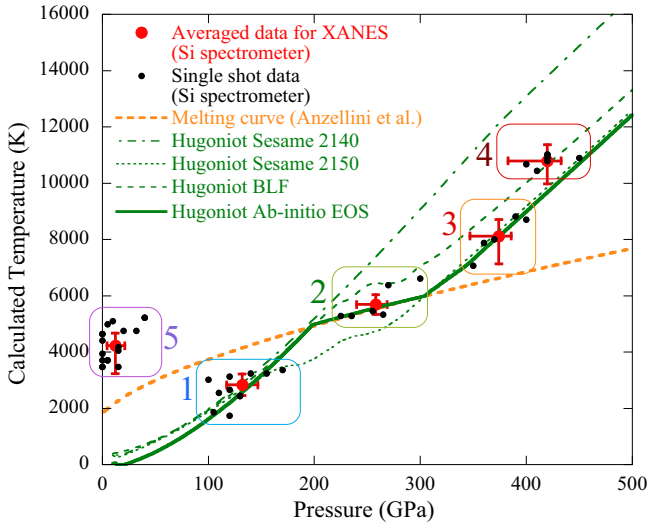


FIG. 3. (Color online) Single-shot pressure as a function of the temperature (black dots), calculated from the VISAR and the SOP measurements when coupled to hydrodynamic simulations. The Hugoniot curves of the SESAME 2140, SESAME 2150, BLF, and the *ab initio* EOS are shown as green lines. The new melting curve of iron by Anzellini *et al.* [4] is shown for reference. The averaging of a group of data for XANES extraction is also shown.

a new EOS table based on *ab initio* molecular dynamics simulations. This table extends to the lower pressures and to the liquid phase, the tabulation of the *ab initio* simulation results published previously in Bouchet *et al.* [2]. This EOS presents the advantage of a high pressure melting curve in agreement with the latest experimental data [4] that are in turn consistent with the *ab initio* results. We also see in Fig. 3 that this EOS is consistent with the 2150 SESAME EOS in the liquid phase. Overall, this *ab initio* EOS is very similar to the SESAME 2150 EOS without the fcc phase extending to high pressures.

As our procedure to extract the pressure and temperature depends on the choice of the EOS, we have tested the sensitivity of the analysis by using three different EOS in the one-dimensional (1D) hydrodynamics simulation (SESAME 2150, SESAME BLF, and the updated *ab initio* EOS). Figure 4 shows the resulting pressure and temperature profiles within the iron sample and at experimental conditions close to the melting curve. We note that the pressure and temperature are uniform and homogeneous along the iron thickness and that the pressure has relatively little sensitivity to the choice of EOS. For the temperature, it leads to a more important uncertainty, up to ∼500 K in the present case at conditions close to the melting curve, when comparing the BLF and the SESAME 2150 to the *ab initio* EOS. To further improve our

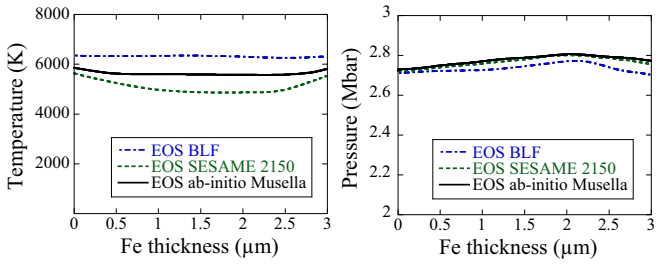


FIG. 4. (Color online) Calculated temperature and pressure profiles in iron from hydrodynamic simulations (code MULTI [31]) using three different EOS (SESAME 2150, BLF, and the *ab initio* EOS) and obtained for an intensity of $5\times10^{12}$ W/cm$^2$.

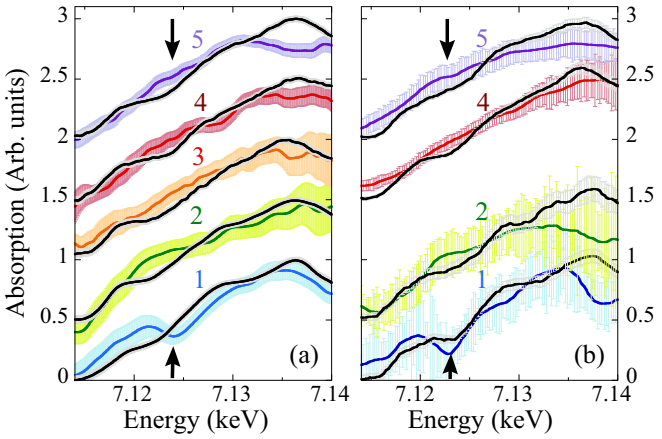


FIG. 5. (Color online) (a) XANES spectra with error ranges arising from photon statistics measured at various conditions (colored lines) and compared to spectra recorded at ambient conditions on bcc iron prior to shot (black lines). Groups of samples labeled from 1 to 5 as shown in Fig. 3 corresponding, for the Si crystal spectrometer, to average values of (1) 11.25 g/cc-2780 K-130 GPa, (2) 12.45 g/cc-5680 K-260 GPa, (3) 13.5 g/cc-8120 K-380 GPa, (4) 13.8 g/cc-10 800 K-420 GPa, and (5) 6 g/cc-4180 K-12 GPa. (b) Corresponding spectra obtained with the quartz crystal.

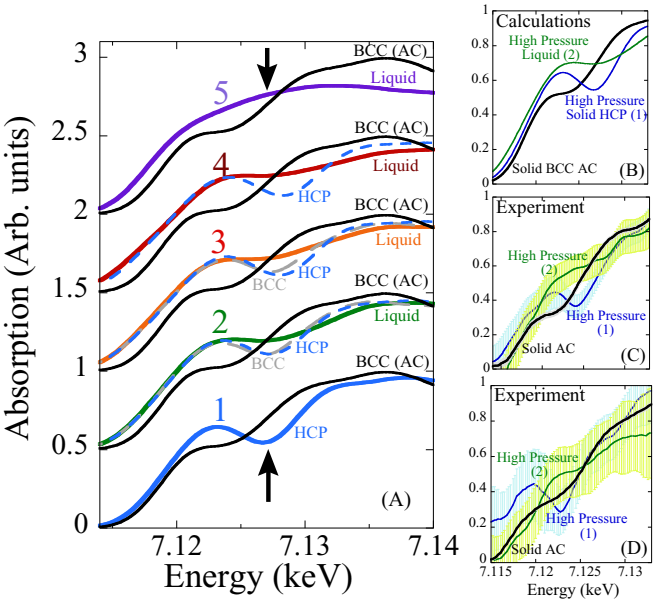


FIG. 6. (Color online) (a) *Ab initio* calculated XANES spectra of liquid Fe (full lines), hcp, and bcc Fe (dotted lines) phases compared to solid bcc Fe at ambient conditions (AC) (black lines). XANES spectra are calculated at the same temperatures and pressures than of the experimental groups, labeled from 1 to 5 (see Fig. 3) with (1) 11.25 g/cc-2780 K-130 GPa, (2) 12.45 g/cc-5680 K-260 GPa, (3) 13.5 g/cc-8120 K-380 GPa, (4) 13.8 g/cc-10 800 K-420 GPa, and (5) 6 g/cc-4180 K-12 GPa. (b) Zoom of the pre-edge region of the calculated XANES spectra of bcc iron at ambient conditions AC (black line), solid hcp Fe at 130 GPa (blue line), and liquid Fe at 260 GPa (green line). (c) Experimental XANES spectra obtained with the Si crystal spectrometers diagnostic at the same conditions. (d) Experimental XANES spectra obtained with the quartz spectrometer at similar conditions.

procedure, we have included such variation of the pressure and temperature induced by the EOS into the error bars calculation. We have estimated each single-shot error bars ($\Delta P_i$, $\Delta T_i$) taking into account the sensibility to the choice of equation of state in addition to the timing uncertainty between the laser and the x-ray FEL probe (measured shot-to shot with ~30 ps accuracy) and the shock velocity uncertainties (~5%). Finally, single-shot measurements are averaged grouping shots sampling similar pressures and temperatures to obtain reliable XANES spectra for five ($P$,$T$) conditions (see Fig. 3). The total error bar ($\Delta P$, $\Delta T$) associated with each of the five averaged ($P$,$T$) conditions are corresponding to the quadratic sum of each single-shot error bars ($\Delta P_i$, $\Delta T_i$).

### B. X-ray absorption spectroscopy (XANES)

Figures 5(a) and 5(b) show the complete set of measured XANES spectra for the thin Si crystal spectrometer (a) and the quartz spectrometer (b). The data sets provided by the two independent spectrometers are consistent. The XANES spectra are obtained by averaging from 5 to 19 single-shots acquisitions at similar thermodynamic conditions. The uncertainty ranges of spectra are calculated using photon statistic [24]. The XANES spectra at ambient conditions are measured just before the shock for each targets and are extracted following the same procedure as the shock XANES spectra, and averaged over the same group of data. They are systematically displayed for each pressure and temperature in Figs. 5 and 6. These ambient conditions spectra provide a test of the variability of the XANES spectra in the course of the experiment showing a good reproducibility. The different qualities of the ambient conditions XANES spectra are related to the photon statistics (number of accumulated shots and integration areas on each spectrometer). Furthermore, we point out that the body cubic center (bcc) spectra obtained at ambient conditions are in good agreement with standard measurements at synchrotron facilities [15].

The XANES spectrum at 130 GPa (±13)-2780 K (±230) (group 1) shows a strong structuration in the pre-edge region, around 7.12 keV, indicated by arrows in Fig. 5. At all the other conditions, at 260 GPa (±29)-5680 K (±700), 380 GPa (±30)-8120 K (±1400), 420 GPa (±50)-10 800 K (±1390), and at 12 GPa (±8)-4180 K (±350) (groups 2, 3, 4, and 5 in Fig. 5), we systematically observe the modification of the pre-edge region, characterized by the disappearance of the minimum around 7.12 keV, as well as by a change of the global slope of the rising edge.

## III. DISCUSSION

### A. Interpretation of x-ray absorption spectra

In order to better interpret the data, XANES spectra were calculated at the same pressure and temperature conditions as in the experiment simulating the different phases at each condition. This is possible due to the limited number of particles used in the simulation, around 150 depending on the phase considered. The calculated XANES spectra for a given phase were obtained by *ab initio* molecular dynamics simulation (ABINIT code) based on the PBE parametrization

of the generalized gradient formulation of density functional theory. The XANES spectra at the iron $K$ edge were calculated using linear response theory on several snapshots at the given pressure and temperature. The methodology of these calculations is further described in Ref. [16]. Figure 6(a) shows the calculated XANES spectra obtained considering a solid hexagonal close packed (hcp), a solid body cubic centered (bcc) phase, or molten Fe. In Figs. 6(b), 6(c), and 6(d) we present a zoom in the pre-edge region of the experimental and calculated XANES spectra obtained at ambient condition together with the 130 GPa-2780 K and the 260 GPa-5680 K experimental data (groups 1 and 2).

In Figs. 5(a) and 5(b) the XANES spectrum at 130 GPa (±13)-2780 K (±230) (group 1) presents a strong structuration with a pre-edge at 7.12 keV that was identified as an effect of the hybridization of the $3d$-$4p$ bands [17]. For iron, this feature can be associated with the hcp phase that has been well documented for instance at 20 and 78 GPa and predicted to remain in hcp iron up to the highest pressures [15,16,32]. Indeed, the calculated XANES spectra of hcp iron at 260, 380, and 420 GPa in Fig. 5 show the persistence of this strong pre-edge structure consisting of a minimum of absorption between 7.12 and 7.13 keV. In contrast, the XANES spectra calculated for liquid iron at the same pressure and temperature show that this feature disappears. This modification of the pre-edge is the signature of a change of the electronic unoccupied density of state. The pre-edge of Fe $K$ edge is generally ascribed to the $1s$-$3d$ quadrupole transition, much weaker than the $1s$ to $4p$ dipole transition driving the main $K$-edge transition [17,33]. In iron, the distortion from centrosymmetry allows the $4p$ orbitals to mix with the $3d$ orbitals (hybridization) and thus the observation of this pre-edge feature. For this reason, pre-edges in XANES are highly sensitive to the local ionic structure and are commonly used to determine local geometric structure as well as coordination number, usually determined by EXAFS techniques [33]. Calculations of the Fe $p$-projected electronic density of state suggest that this pre-edge feature is much less visible in liquid Fe than in hcp Fe [16,17] at a given temperature and density (see Fig. 6). We emphasize that this damping of the pre-edge structure cannot be ascribed to a pure thermal effect as shown for example in Fig. 6(b) in which bcc, hcp, and liquid Fe were calculated at the same temperature. This effect might be more sensitive than the global loss of structuration in the extended x-ray absorption spectra, which can be inadequate because of the persistence of a short-range order in the liquid phase [34,35]. Identical modifications of the pre-edge structure of iron have been reported in XANES measurements of molten iron in previous diamond-anvil-cells experiments [14,32]. Moreover, we note that at 380 and 420 GPa along the Hugoniot (groups 3 and 4) and 12 GPa on the release adiabat (group 5), temperatures are far above any measured or calculated melting curve of iron. We therefore argue that, based on *ab initio* calculations and on previous literature data on laser-heated diamond cell experiments, the simplest interpretation of the structure change in the pre-edge consisting in the attenuation of the minimum between 7.12 and 7.13 keV observed in our data is due to melting of iron. In this interpretation, iron is identified as hcp at 130 GPa-2780 K condition (group 1, in blue in Fig. 5) and as mostly liquid Fe at 260 GPa-5680 K (group 2, in green in Fig. 5). This suggests that the melting line of iron would have already been crossed at 260 GPa (± 29)-5680 K (± 700) along the principal Hugoniot of Fe.

### B. Iron phase diagram and discussion

If we consider that the change of the pre-edge in the XANES spectra allows us to distinguish solid or liquid iron, we can infer the nature of iron at the indicated points on the iron phase diagram in Fig. 7. This is shown together with previous experimental and theoretical data. Our interpretation indicates that at 260 GPa iron would already be molten. Optical diagnostics coupled with hydrodynamic simulations give an associated temperature of 5680 K (±700) suggesting that the melting curve of iron is below 5680 K at 260 GPa (upper limit of 5915 K deduced from the error bars). Once error bars are taken into account, the observation of solid or liquid iron along the Hugoniot using the XANES criterion is consistent with most existing data or models about iron melting [1,2,4,6,11,12] except for shock wave measurements based on self-emission diagnostics [8–10], which gave a Hugoniot melting temperature of 6700 K at 260 GPa [8].

A possibility for explaining this discrepancy is that methods probing bulk samples, such as x-ray absorption used in the present study, could be less sensitive to shock overheating than optical surface diagnostics that probe only the shock front. Indeed, shock overheating occurs when the temperature rises faster than the rate of atom rearrangement required for phase transition [5]. While optical diagnostics may probe time scales corresponding to the rise of temperature in the shock

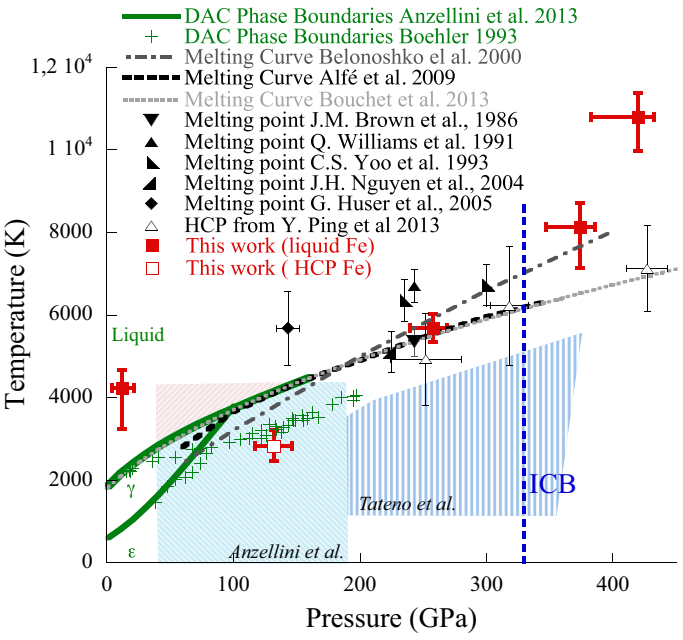


FIG. 7. (Color online) Iron phase diagram: Our results (red open squares for solid hcp and red full square for liquid Fe) are compared with previous results and extrapolation obtained in the literature from diamond-anvil-cell compression [4,6,36], shock-waves experiments [8–13], and *ab initio* simulations [1–3]. The ICB pressure of 330 GPa is shown with a dashed blue line.

front and therefore be more sensitive to kinetics, here we probe the bulk of the material a few hundreds of picoseconds after the shock breakout from Fe, when the overall sample is under compression and still presents uniform pressure and temperature. A more advanced answer to this question could be given by measuring directly the temperature from both optical and x-ray diagnostics as well as simultaneously detecting the melting with x-ray diagnostics.

To conclude, our results open new perspectives for performing ultrafast x-ray absorption measurements on laser compressed materials. We emphasize that this study provides new structural data along the principal Hugoniot of laser compressed iron by providing x-ray absorption measurements at the Fe $K$ edge.

## ACKNOWLEDGMENTS

We acknowledge R. Torchio, P. Mounaix, D. Antonangeli, and D. Cabaret for helpful discussions. We thank our reviewers and the editor who helped to considerably improve the manuscript. This work is supported by the French Agence Nationale de la Recherche (ANR) with the ANR IRONFEL and Planetlab. This work was performed at the Matter at Extreme Conditions (MEC) instrument of LCLS, supported by the DOE Office of Science, Fusion Energy Science under Contract No. SF00515. This work was also supported by LCLS, a National User Facility operated by Stanford University on behalf of the US Department of Energy, Office of Basic Energy Sciences.

[1] D. Alfè, Phys. Rev. B **79**, 060101 (2009).
[2] J. Bouchet, S. Mazevet, G. Morard, F. Guyot, and R. Musella, Phys. Rev. B **87**, 094102 (2013).
[3] A. B. Belonoshko, R. Ahuja, and B. Johansson, Phys. Rev. Lett. **84**, 3638 (2000).
[4] S. Anzellini, A. Dewaele, M. Mezouar, P. Loubeyre, and G. Morard, Science **340**, 464 (2013).
[5] S. N. Luo and T. J. Ahrens, Phys. Earth Plan. Int. **143-144**, 369 (2004).
[6] R. Boehler, Nature (London) **363**, 534 (1993).
[7] T. J. Ahrens, K. G. Holland, and G. Q. Chen, Geophys. Res. Lett. **29**, 1150 (2002).
[8] Q. Williams, E. Knittle, and R. Jeanloz, J. Geophys. Res. **96**, 2171 (1991); Q. Williams, R. Jeanloz, J. Bass, B. Svendsen, and T. J. Ahrens, Science **236**, 181 (1987).
[9] C. S. Yoo, N. C. Holmes, M. Ross, D. J. Webb, and C. Pike, Phys. Rev. Lett. **70**, 3931 (1993).
[10] G. Huser, M. Koenig, A. Benuzzi-Mounaix, E. Henry, T. Vinci, B. Faral, M. Tomasini, B. Telaro, and D. Batani, Phys. Plasma **12**, 060701 (2005).
[11] J. M. Brown and R. G. McQueen, J. Geophys. Res. **91**, 7485 (1986).
[12] J. H. Nguyen and N. C. Holmes, Nature (London) **427**, 339 (2004).
[13] Y. Ping, F. Coppari, D. G. Hicks, B. Yaakobi, D. E. Fratanduono, S. Hamel, J. H. Eggert, J. R. Rygg, R. F. Smith, D. C. Swift, D. G. Braun, T. R. Boehly, and G. W. Collins, Phys. Rev. Lett. **111**, 065501 (2013).
[14] C. Marini, F. Occelli, O. Mathon, R. Torchio, V. Recoules, S. Pascarelli, and P. Loubeyre, J. Appl. Phys. **115**, 093513 (2014).
[15] O. Mathon, F. Baudelet, J. P. Itié, A. Polian, M. d'Astuto, J. C. Chervin, and S. Pascarelli, Phys. Rev. Lett. **93**, 255503 (2004).
[16] S. Mazevet, V. Recoules, J. Bouchet, F. Guyot, M. Harmand, A. Ravasio, and A. Benuzzi-Mounaix, Phys. Rev. B **89**, 100103(R) (2014).
[17] A. T. Raji and S. Scandolo, High Pressure Res. **33**, 119 (2014).
[18] A. Benuzzi-Mounaix, F. Dorchies, V. Recoules, F. Festa, O. Peyrusse, A. Levy, A. Ravasio, T. Hall, M. Koenig, N. Amadou, E. Brambrink, and S. Mazevet, Phys. Rev. Lett. **107**, 165006 (2011).
[19] A. Lévy, F. Dorchies, A. Benuzzi-Mounaix, A. Ravasio, F. Festa, V. Recoules, O. Peyrusse, N. Amadou, E. Brambrink, T. Hall, M. Koenig, and S. Mazevet, Phys. Rev. Lett. **108**, 055002 (2012).
[20] A. Denoeud, A. Benuzzi-Mounaix, A. Ravasio, F. Dorchies, P. M. Leguay, J. Gaudin, F. Guyot, E. Brambrink, M. Koenig, S. Le Pape, and S. Mazevet, Phys. Rev. Lett. **113**, 116404 (2014).
[21] M. Harmand, F. Dorchies, O. Peyrusse, D. Descamps, C. Fourment, S. Hulin, S. Petit, and J. J. Santos, Phys. Plasma **16**, 063301 (2009).
[22] The principal Hugoniot defines a unique trajectory in $(P,T)$ space relating an initial and final states by conservation of energy and momentum.
[23] Ya. B. Zel'dovich and Yu. P. Raizer, *Physics of Shock Waves and High-Temperature Hydrodynamic Phenomena* (Academic Press, New York, 1968).
[24] J. Gaudin, C. Fourment, B. I. Cho, K. Engelhorn, E. Galtier, M. Harmand, P. M. Leguay, H. J. Lee, B. Nagler, M. Nakatsutsumi, C. Ozkan, M. Störmer, S. Toleikis, Th. Tschentscher, P. A. Heimann, and F. Dorchies, Sci. Rep. **4**, 4724 (2014).
[25] D. Zhu, M. Cammarata, J. M. Feldkamp, D. M. Fritz, J. B. Hastings, S. Lee, H. T. Lemke, A. Robert, J. L. Turner, and Y. Feng, Appl. Phys. Lett. **101**, 034103 (2012).
[26] M. Koenig, F. Philippe, A. Benuzzi-Mounaix, D. Batani, M. Tomasini, E. Henry, and T. Hall, Phys. Plasmas **10**, 3026 (2003).
[27] A. Ravasio, G. Gregori, A. Benuzzi-Mounaix, J. Daligault, A. Delserieys, A. Ya. Faenov, B. Loupias, N. Ozaki, M. Rabec le Gloahec, T. A. Pikuz, D. Riley, and M. Koenig, Phys. Rev. Lett. **99**, 135006 (2007).
[28] J. Barnes and J. Rood (Los Alamos National Laboratory), documentation for SESAME EOS 2140 for Fe (1973) (unpublished).
[29] G. I. Kerley, Sandia National Laboratories Report No. SAND93-0027 (1993) (unpublished).
[30] A. V. Bushman, I. V. Lomonosov, and V. E. Fortov, *Equations of State of Metals at High Energy Densities* (Institute of Chemical Physics, Russian Academy of Sciences, Chernogolovka, 1992) (in Russian).
[31] R. Ramis, R. Schmalz, and J. Meyer-ter-Vehn, Comput. Phys. Commun. **49**, 475 (1988).
[32] R. Boehler, H. G. Musshoff, R. Ditz, G. Aquilanti, and A. Trapananti, Rev. Sci. Instrum. **80**, 045103 (2009).

[33] S. DeBeer George, T. Petrenko, and F. Neese, J. Phys. Chem. A **112**, 12936 (2008).

[34] A. Mancic, A. Lévy, M. Harmand, M. Nakatsutsumi, P. Antici, P. Audebert, P. Combis, S. Fourmaux, S. Mazevet, O. Peyrusse, V. Recoules, P. Renaudin, J. Robiche, F. Dorchies, and J. Fuchs, Phys. Rev. Lett. **104**, 035002 (2010).

[35] F. Dorchies, A. Lévy, C. Goyon, P. Combis, D. Descamps, C. Fourment, M. Harmand, S. Hulin, P. M. Leguay, S. Petit, O. Peyrusse, and J. J. Santos, Phys. Rev. Lett. **107**, 245006 (2011).

[36] S. Tateno, K. Hirose, Y. Ohishi, and Y. Tatsumi, Science **330**, 359 (2010).